Eur. Phys. J. C (2023) 83:397
https://doi.org/10.1140/epjc/s10052-023-11558-z

THE EUROPEAN PHYSICAL JOURNAL C

Regular Article - Theoretical Physics

Regularizing the JNW and JMN naked singularities

Kunal Pal[1,a], **Kuntal Pal**[1,b], **Pratim Roy**[2,3,c], **Tapobrata Sarkar**[1,d]

[1] Department of Physics, Indian Institute of Technology Kanpur, Kanpur 208016, India
[2] Harish-Chandra Research Institute, Chhatnag Road, Jhunsi, Prayagraj 211019, India
[3] Homi Bhabha National Institute, Training School Complex, Anushaktinagar, Mumbai 400094, India

Received: 29 March 2023 / Accepted: 24 April 2023 / Published online: 12 May 2023

Abstract We extend the method of Simpson and Visser (SV) of regularizing a black hole spacetime, to cases where the initial metric represents a globally naked singularity. We choose two particular geometries, the Janis–Newman–Winicour (JNW) metric representing the solution of an Einstein-scalar field system, and the Joshi–Malafarina–Narayan (JMN) metric that represents the asymptotic equilibrium configuration of a collapsing star supported by tangential pressures as the starting configuration. We illustrate several novel features for the modified versions of the JNW and JMN spacetimes. In particular, we show that, depending on the values of the parameters involved the modified JNW metric may represents either a two way traversable wormhole or it may retain the original naked singularity. On the other hand, the SV modified JMN geometry is always a wormhole. Particle motion and observational aspects of these new geometries are investigated and are shown to posses interesting features. We also study the quasinormal modes of different branches of the regularized spacetime and explore their stability properties.

1 Introduction

Despite being the most successful theory of gravity till date, it is widely believed that general relativity (GR) [1] may break down in high curvature regimes, where it will be replaced by an yet unknown theory of quantum gravity. For this reason, the final fate of a gravitational collapse, starting from some well behaved set of initial data is still an open problem, as the analysis carried out in the classical (or effectively semiclassical) theory may received important quantum corrections in the strong gravity regime. In this context, two important questions are known to arise. First, if the regular interior of a collapsing star in realistic situations produce a spacetime singularity, which is specified by a diverging curvature scalar, and secondly, whether this singularity is visible to an asymptotic observer. The latter is thought to be prohibited by the cosmic censorship conjecture (CCC) of Penrose [2], which is yet to be proved in full generality. In the absence of a fully accepted theory of quantum gravity, a popular line of research to study the above mentioned problems is to construct a model of 'regular black holes,' where the singularity is replaced by a region of regular curvature. On the other hand, the notion of a 'horizonless compact object' with or without a singularity, like a wormhole (WH) [3–10], a naked singularity (NS) etc., has also gained considerable attention in the literature. Although the presence of a wormhole throat may violate the standard classical energy conditions of general relativity [3], hinting towards the presence of exotic matter, there are examples of WH solutions of modified gravity that satisfy all or some of the energy conditions [4–8]. On the other hand, the presence of a NS without an event horizon would violate the CCC, there are well studied models in the literature, where the end states of a viable collapse process produces a NS, and therefore it is fair to say that a firm conclusion is yet to be reached in the matter.

Starting from the seminal work of Bardeen [11], there are abundant models of regular black holes which are constructed either from a purely phenomenological point of view, or as solutions of an effective semiclassical gravity theory (for a review and further references, see [12]). The basic idea of these kinds of phenomenological models is to replace the Schwarzschild mass by some general family of mass functions, that would render the curvature scalars finite everywhere in the spacetime. Though this looks promising at first sight, there are many models of regular black holes that have

[a] e-mail: kunalpal@iitk.ac.in (corresponding author)
[b] e-mail: kuntal@iitk.ac.in
[c] e-mail: pratimroy@hri.res.in
[d] e-mail: tapo@iitk.ac.in

an inner Cauchy horizon, and its instability under mass inflation can be problematic for realistic model building (see [13] and references therein). In view of the above discussions, we are led to consider an interesting one parameter class of models for regularizing the Schwarzschild singularity, that was proposed recently by Simpson and Visser (SV) [14]. Here, the central singularity was replaced by a regular region, that can be timelike, null, or spacelike, depending on the parameter involved in the geometry, and the global geometry represents either a traversable WH or a regular BH with one horizon. Such models, dubbed as 'black-bounce' spacetimes, not only resolve the Schwarzschild singularity, but also provide a link between two different classes of spacetime structures, namely the BH and the WH, and therefore is a promising way of further constructing regular black holes and resolving the singularity problem of classical GR. See [15–27] for a selection of recent works in this direction.

In view of the above discussions, an interesting question concerns the behaviour of globally naked singularities that can be regularized following the SV procedure. It is this issue that we address in this paper. Here, our purpose is to extend the method of SV and construct regular solutions starting from a globally naked singularity, and in the process unify two different classes of metrics, namely the WH and NS. To this end, we first apply the SV regularization scheme to the Janis–Newman–Winicour (JNW) [28,29] class of spacetimes which have a naked curvature singularity at a finite radial location, and reduces to the Schwarzschild black hole for a particular limit of the parameters involved. We construct a deformed JNW metric that interpolates between a BH, WH and NS for different ranges of the parameters. As a second example, we construct a similar deformation of the Joshi–Malafarina–Narayan (JMN) [30] spacetime, that contains a central NS and is known to be a result of gravitational collapse of regular initial data. In the following sections, we discuss the resulting metrics and show that these are indeed rich in terms of global spacetime structures and observational aspects. Further, we discuss the quasinormal modes (QNMs) of the regularized JNW metric using the WKB approach [51–53] concentrating on the wormhole branch, and comment on the stability of the spacetime, particularly when approaching the NS branch by changing the SV parameter. Indeed it is an important task to check the viability of any WH model, by testing the stability of the corresponding metric against small perturbations by calculating the related QNM spectra [54–59]. As the resulting SVJNW spacetime can interpolate between a WH and a NS depending on the relative parameters involved, our main motivation to this end is to study how the stability of the WH branch changes as we parametrically move towards the NS branch. Since it is difficult to directly apply the semiclassical WKB method for a generic NS metric [60], our result, that points towards a decrease in stability of the spacetime towards the NS branch, seems to be of importance in the context of the stability of a NS spacetime [61].

We always work in units where the Newton's gravitational constant and the speed of light are set to unity.

Note Added: While this draft was being finalised, the recent paper [49] appeared, which has partial overlap with the results presented in Sect. 2 of this work. However, the final metric considered in [49] is slightly different than that we considered due to a different coordinate system chosen.

2 Deformed Janis–Newman–Winicour solution

The Janis–Newman–Winicour metric [28,29] is a static, spherically symmetric solution of the Einstein field equations in the presence of a minimally coupled scalar field, and is given by the line element

$$ds^2 = -\left(1-\frac{b}{r}\right)^{\gamma} \mathrm{d}t^2 + \left(1-\frac{b}{r}\right)^{-\gamma} \mathrm{d}r^2 + \left(1-\frac{b}{r}\right)^{1-\gamma} r^2 \mathrm{d}\Omega^2. \tag{1}$$

The parameters γ and b appearing in the JNW metric are related to the ADM mass M and the scalar charge q by the relations

$$\gamma = \frac{2M}{b}, \quad b = 2\sqrt{M^2+q^2}. \tag{2}$$

In the limit of vanishing scalar charge $q \to 0$, the JNW solution reduces to the Schwarzschild solution. In the general case, with $q \neq 0$, and real, it can be seen from Eq. (2) that $\gamma < 1$. This fact also indicates that the JNW metric is only valid up to the coordinate location $r = b$. It can also be checked that for $\gamma < 1$, this metric has a curvature singularity at $r = b$, and since the metric does not possess any event horizon, it is a naked singularity [31]. On the other hand, when the scalar charge q is imaginary such that $\gamma > 1$, this metric represents a symmetric traversable WH with two asymptotically flat regions [32,33].

Now we apply the SV method via the replacement $r \to \sqrt{r^2+c^2}$, without modifying the form dr (in which case it will simply be an uninteresting overall coordinate transformation) in the JNW solution, and the resulting metric becomes

$$ds^2 = -\left(1-\frac{b}{\sqrt{r^2+c^2}}\right)^{\gamma} \mathrm{d}t^2 + \left(1-\frac{b}{\sqrt{r^2+c^2}}\right)^{-\gamma} \mathrm{d}r^2 + \left(1-\frac{b}{\sqrt{r^2+c^2}}\right)^{1-\gamma} \left(r^2+c^2\right) \mathrm{d}\Omega^2. \tag{3}$$

Here c (not to be confused with the speed of light), the SV parameter, is a real and positive quantity having dimensions of length. The range of coordinates, other than that of r are

same as before, and the range of r depends upon the relative values of c and b, as we explain below in detail. Also, it can readily be seen that the original symmetries and the asymptotic properties of the JNW metric are preserved with the new one. We will get back the JNW metric in the limit $c \to 0$ and the SV metric (i.e., the deformed Schwarzschild metric) in the limit $\gamma \to 1$.

Now we elaborate upon the metric of Eq. (3) (which we shall call the SV-JNW solution from now on) for different parameter ranges. For this, it will be useful to define a coordinate transformation $k^2 = r^2 + c^2$, doing which we get

$$ds^2 = -\left(1-\frac{b}{k}\right)^{\gamma} \mathrm{d}t^2 + \left(1-\frac{b}{k}\right)^{-\gamma} \frac{k^2}{k^2-c^2}\mathrm{d}k^2 + \left(1-\frac{b}{k}\right)^{1-\gamma} k^2 \mathrm{d}\Omega^2. \tag{4}$$

To gain more insight into the structure of the metric, we use another coordinate transformation

$$R^2 = \left(1-\frac{b}{k}\right)^{1-\gamma} k^2, \tag{5}$$

after which the final form of the metric is,

$$ds^2 = -\left(1-\frac{b}{k(R)}\right)^{\gamma} \mathrm{d}t^2 + \left(1-\frac{b}{k(R)}\right)^{-\gamma} \frac{k(R)^2}{k(R)^2-c^2} \left(\frac{1}{D(k)^2\left(1+\frac{b(1-\gamma)}{2(k-b)}\right)^2}\right) \mathrm{d}R^2 + R^2 \mathrm{d}\Omega^2, \tag{6}$$

and we have defined $D(k) = \left(1-\frac{b}{k}\right)^{\frac{1-\gamma}{2}}$. Since Eq. (5) can be inverted in principle to obtain k in terms of the new variable R, we have retained its implicit dependence. To gain insights into this metric, we now compare this to the canonical Morris–Thorne WH [34]

$$ds^2 = -\exp(2\Phi)\mathrm{d}t^2 + \frac{1}{1-\frac{B(R)}{R}}\mathrm{d}R^2 + R^2\mathrm{d}\Omega^2, \tag{7}$$

where $B(R)$ is the shape function and $\Phi(R)$ is the redshift function. For our metric the shape function is given by

$$B(k(R)) = R\left[1-\left(1-\frac{b}{k}\right)\left(1-\frac{c^2}{k^2}\right)\left(1+\frac{b(1-\gamma)}{2(k-b)}\right)\right]. \tag{8}$$

From the form of the redshift function g_{tt} in Eq. (4), we can see that it vanishes at $k_1 = b$. Similarly, The g^{RR} component of the above metric in Eq. (6) has two zeros, respectively at $k_2 = c$, and $k_3 = \frac{b}{2}(\gamma+1)$. Furthermore, the equation for the radial null curves for the metrics in the R, t coordinates are given by

$$\frac{dR}{dt} = \left[\left(1-\frac{b}{k}\right)^{\gamma} \frac{(k^2-c^2)\Big(2(k-b)+b(1-\gamma)\Big)}{4k^3(k-b)}\right]^{1/2}. \tag{9}$$

Thus, depending upon the nature of the parameters involved in the metric, we can have several interesting cases here, which we now detail. First we shall consider the cases with $\gamma < 1$.

• $\gamma < 1$ and $b < c$: Here, $k_3 < k_1$ and hence the root k_3 does not play any significant role, since the metric is not valid up to the coordinate value corresponding to k_3. In this case, it can readily be seen that the original domain of validity of the JNW metric (up to $r \geq b$) has changed, and the metric can be continued from $r = \infty$ to $r = -\infty$, through $r = 0$. The metric then represents a traversable wormhole, with a timelike throat at $r = 0$, connecting two asymptotically flat regions. This is very different from the usual JNW solution, where no WH branch exists for $\gamma < 1$. For completeness, we explicitly check that the conditions for a traversable wormhole [3] are satisfied here:

(i) Absence of horizons: This can be seen from the metric written in Eq. (4), from which it is evident that the spacetime does not contain any horizon as long as $b < c$ is satisfied.

(ii) Flaring out condition: This condition satisfied by a traversable wormhole embodies the fact that the throat is the location of minimum area (see [35] for a detailed discussion). Mathematically, the flaring out condition implies that $A'(r = r_0) = 0$, $A''(r = r_0) > 0$, where the prime denotes a derivative with respect to the radial coordinate. For the metric of Eq. (3), we note that the area of the two sphere is $A(r) = \left(1-\frac{b}{\sqrt{r^2+c^2}}\right)^{1-\gamma}(r^2+c^2)$, and hence $A'(r = r_0) = 0 \implies r_0 = 0$, i.e., we have a stationary point of the area of the spherical surface at the throat $r = r_0 = 0$. To check that this represents a minimum we only need to note that $A''(r = r_0) = \frac{2\left(2c-b(1+\gamma)\right)}{c(1-\frac{b}{c})^{\gamma}}$. Thus as long as the condition $b < c$ satisfied $A''(r = r_0) > 0$, and we see that the area is indeed minimum at the location of the throat, and that the flaring out condition is indeed satisfied.

(iii) Non-singular nature: To show that the resulting geometry is non singular everywhere – which is required for the metric to represent a wormhole geometry, we calculate the curvature scalars. The Ricci scalar in this case $R \sim (1-\frac{b}{\sqrt{r^2+c^2}})^{-2}$, where we have omitted some factors, not important for the present purpose. From this, we see that it is indeed finite everywhere, including $r = 0$ and $r = b$. Similarly, the Kretschmann scalar $K \sim (1-\frac{b}{\sqrt{r^2+c^2}})^{-4}$ which is also finite everywhere.

• $\gamma < 1$ and $b > c$: Here, the range of the radial coordinate is restricted to $\sqrt{b^2-c^2} < r < \infty$, a condition analogous to that in the original JNW metric. The Ricci scalar, given by $R \sim (1-\frac{b}{\sqrt{r^2+c^2}})^{-2}$, diverges in the limit $r \to \sqrt{b^2-c^2}$ (the same conclusion can be shown to be valid for the Kretschmann scalar curvature). On the other hand, from the expression of the metric, it can be seen that there is no possibility an event horizon at the location of the curvature singularity. So, as in the case of the original JNW metric [31], we conclude that the singularity is not covered by that of an event horizon from a distant observer, and that the spacetime represents a naked singularity for the above parameter ranges.
• $\gamma < 1$ and $b = c$: This is the limiting case of the two earlier ones. As explained above, here the metric consists of a throat (minimum of the local area), and the curvature singularity, all at the location $r = 0$, as well as there is no possibility of an event horizon. So the metric represents a one way wormhole with a singular throat.

Now we examine the solutions for the range $\gamma > 1$. This case is similar to that of the original JNW WH [32,33], although due to the introduction of the parameter c, we will have a richer geometric structure. First note that here $k_3 > k_1$, and in the original coordinate r, the three locations k_is are written as

$$r_1 = \sqrt{b^2-c^2}, \quad r_2 = 0, \quad r_3 = \sqrt{\frac{b^2}{4}(\gamma+1)^2 - c^2}. \quad (10)$$

As before we will consider two cases $b > c$ and $b < c$ and their limiting case.
• $b < \frac{b}{2}(\gamma+1) < c$: Here, we consider only $r_2 = 0$ from Eq. (10), which is the only real one in this case. Again, we see that the region of validity of the metric is changed to the range from $r = -\infty$ to $r = \infty$. In this case, the metric represents a traversable wormhole with a throat at $r = 0$. One can check the validity of the WH features here, but we omit the details for brevity.
• $b < c < \frac{b}{2}(\gamma+1)$: In this case, the value of γ is such that only r_3 in Eq. (10) is real. We can immediately see that this metric represents a traversable WH with a throat at r_3, with similar arguments as before.

Finally note that there is no possibility of any NS branch here, as even in the case $c < b < \frac{b}{2}(\gamma+1)$, the metric represents a WH, since the metric is still valid up to r_3. So we can conclude that the NS is fully regularized here, following the SV method.

2.1 Photon motion in SV-JNW background

Now we discuss the motion of a photon in the SV-JNW background, and the resulting shadow structure of the metric in Eq. (3). Since the metric is spherically symmetric, the structure of the null geodesics is fairly simple, and here our main goal will be to compare and contrast this spacetime with its two limits, namely the SV metric ($\gamma \to 1$) and the JNW metric ($c \to 0$) in terms of the effective potential encountered by a photon moving in these three spacetimes.[1] The standard approach to study the null geodesics motion and consequently finding the photon sphere, which are the unstable orbits of light rays, is to use the Hamilton–Jacobi equation. After performing a standard analysis, the effective potential encountered by a photon in a spherically symmetric background can be written as [37]

$$V_{eff}(r) = g_{tt}\frac{C+L^2}{\mathcal{B}(r)}, \quad (11)$$

where g_{tt} represents the temporal component of the metric and $\mathcal{B}(r)$ is its two sphere part. Here, C and L are the Carter's constant and the angular momentum respectively, and both of them are conserved quantities associated with the photon motion. Using the relevant functions from Eq. (3), we get the expression of the effective potential for the photon motion to be

$$V_{eff}(r) = \frac{C+L^2}{r^2+c^2}\left(1-\frac{b}{\sqrt{r^2+c^2}}\right)^{2\gamma-1}. \quad (12)$$

The circular photon orbits can be obtained by imposing the condition of vanishing radial velocity along with the condition for the extremum of the effective potential, $\dot{r} = 0$ and $V'_{eff} = 0$. Typically this extremum turns out to be a maximum, and photon orbits are unstable. Solving this constraint, we obtain the following three solutions,

$$\begin{aligned} &r_1 = 0, \quad r_2 = \sqrt{b^2-c^2}, \quad \text{and} \\ &r_3 = \left\{b^2\left(\frac{1}{4}(2\gamma-1)^2 + (2\gamma-1) + 1\right) - c^2\right\}^{1/2} \\ &\quad = \sqrt{b^2\left(\gamma+\frac{1}{2}\right)^2 - c^2}. \end{aligned} \quad (13)$$

This gives correct result for SV metric ($\gamma \to 1$) [14] and in the limit $c \to 0$, it correctly reduces to the known photon sphere of the JNW metric. Now, depending on the range of the various parameters (b, c, γ), the above three roots give the photon sphere in this spacetime, as we elaborate below. In this section we shall consider only values of $\gamma < 1$.
• Photon motion for $b < c$: As we have discussed above, in this case the spacetime is a wormhole (WH) with a throat at $r = 0$. We can directly see from Eq. (13) that in this case, the solution r_2 is not real, and the parameter range the other two solutions might be relevant here. In this context, we note

[1] The observational features of the above two cases are well studied in the literature for example see [14] for SV metric and [36,37] for the JNW metric.

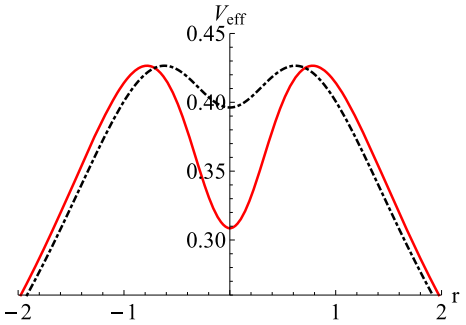

Fig. 1 V_{eff} for the WH branch when $c > b$. The solid red curve represents the case with $c = 1.1$, and the dotted black is with $c = 1.2$. For both, $b = 1$, $\gamma = 0.85$, $C = L = 1$

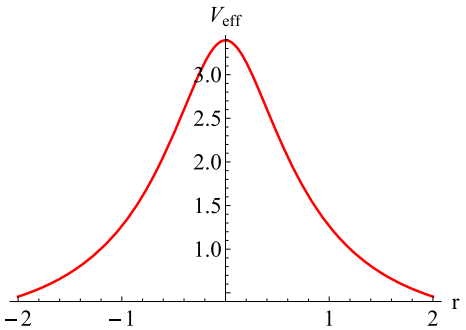

Fig. 2 Plot of the effective potential for the WH case. The solid red curve represents the case with $\gamma = 0.35$ for which maximum of $V_{eff}(r)$ is at r_1. We have set $b = 1$, $c = 1.1$, $C = L = 1$

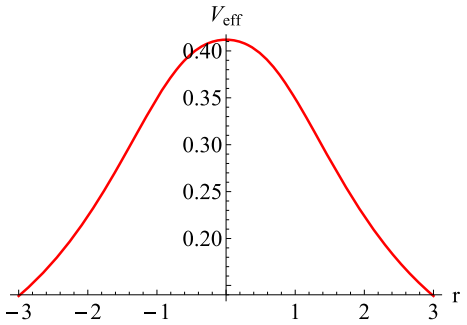

Fig. 3 V_{eff} for the WH case. The curve represents the case with $\gamma = 0.85$ for which maximum of $V_{eff}(r)$ is at r_1. Here, $b = 1$, $c = 1.5$, $C = L = 1$

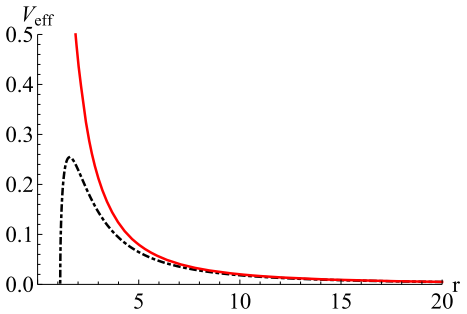

Fig. 4 V_{eff} for the NS case. The solid red curve is with $\gamma = 0.45$, and the dashed black curve is for $\gamma = 0.85$. For both plots, $b = 1.5$, $c = C = L = 1$

that the motion of light in wormhole backgrounds has been widely studied in the literature, see, e.g., [38] and references therein. Here the stand out feature for the wormhole background is the fact that apart from the conventional photon sphere outside the throat, the throat can itself work as a location of the photon sphere (i.e., a location of the maximum of the effective potential), see [39] for details. For our purposes, the two sub-cases are important in this class of solutions, namely whether the third root r_3 is real or not corresponding to some given parameter range.

First, we consider the case when r_3 is real. Then the root r_3 ($> r_1$) can be real only if $\gamma > \frac{1}{2}$. This range of gamma $1/2 < \gamma < 1$ is the same as that of the JNW metric, and when this condition is satisfied, r_3 is a location of photon sphere. The plot of the effective potential is shown in Fig. 1, for two different values of c with fixed $\gamma = 0.85$, $b = 1$. A light ray from our universe will encounter this photon sphere first and will form shadow [40]. Now the interesting case happens if we continue to increase c, such that the value of r_3 saturates.

Next, consider the case where r_3 not real, which can be due to two different reasons. Firstly if $\gamma < 1/2$, then r_3 is not physical for any value of b, c (with $b < c$). In this case, the throat at r_1 acts as the location of the unstable orbits of photon and generates the shadow. We note that this is in contrast to JNW spacetime, where no photon sphere is possible for $\gamma < 0.5$. This case is illustrated in Fig. 2.

On the other hand, even if $\gamma > 1/2$, since γ is always less than unity, there is an upper bound on c for which r_3 can be real. This can be found from setting $\gamma = 1$ in r_3, from which we conclude that if $c > \frac{3b}{2}$, then r_3 is not real, and in this case also r_1 acts as a location of unstable photon orbit, see the plot of the effective potential in Fig. 3.

• Photon motion for $b > c$: In this case, the spacetime itself is valid up to a radial distance $r = \sqrt{b^2 - c^2}$, and it represents a naked singularity at that coordinate location. Clearly, among the three solutions in Eq. (13), the $r_1 = 0$ solution is not relevant here, and since the second solution $r_2 = \sqrt{b^2 - c^2}$ is the location of the curvature singularity itself, it cannot be the physically relevant photon sphere. Importantly however, depending on the range of γ, the solution r_2 decides whether the third solution gives rise to a physically relevant photon sphere or not, since if for some value of γ, it turns out that $r_3 < r_2$, then r_3 is not physical, even if it a real solution.

The allowed range of γ can be found from Eq. (13) to be $\gamma > \frac{1}{2}$, as we are considering the case $b > c$. So in this case, the spacetime has **one photon sphere** at the coordinate location r_3 for $\frac{1}{2} < \gamma < 1$ and **no photon sphere** for $0 < \gamma < \frac{1}{2}$. Note that as long as $\gamma > \frac{1}{2}$, there is no restriction

on the values of b, c except $b > c$, unlike above case, as r_3 will always be real as long as above conditions are satisfied. In Fig. 4, we have shown the effective potential in this case.

Furthermore, unlike the WH case discussed above, here we cannot have a photon sphere for $\gamma < 0.5$, as $r_3 < r_2$ will always be satisfied, and we will have a NS configuration without a photon sphere. In this way the NS branch mimics the behaviour of photons in the JNW metric.

To summarize, the SV-JNW spacetime we have constructed can have one photon sphere (at r_3 or r_1) or can have no photon sphere at all, depending on the relative values of the parameters b and c, as well as that of γ. This behaviour is to be contrasted with the standard JNW metric and the SV metric, which are two particular limits of our metric. To this end, a qualitative comparison of the effective potentials encountered by a massless particles moving in SV, JNW and SV-JNW solutions is given in Fig. 5 (for the SV and SV-JNW solutions, only the WH branches are plotted). In particular, note the contrast between the JNW and SV-JNW cases. Due to the fact that the SV-JNW solution has a WH branch, its effective potential continues into the other universe also. The large $r > 0$ behaviours of all these cases are similar, since all of them are asymptotically Minkowski spacetimes.

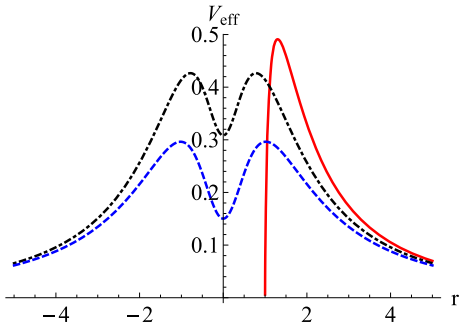

Fig. 5 Effective potentials encountered by a massless particle for the SV (blue dashed curve), JNW (red curve) and SV-JNW (black dot-dashed curve) spacetimes

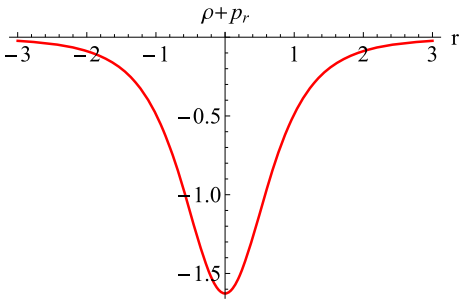

Fig. 6 $\rho + p_r$ for the WH branch with $\gamma = 0.45, c = 1.1, b = 0.1$. The NEC is always violated

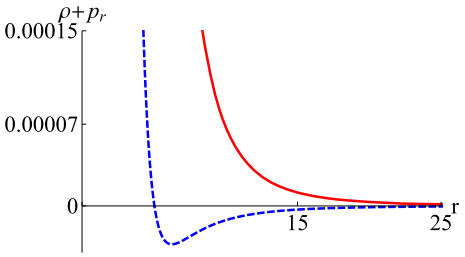

Fig. 7 $\rho + p_r$ for the NS branch. The solid red curve is plotted with $\gamma = 0.25$ which satisfies the NEC, and the dashed blue curve is with $\gamma = 0.85$ for which the NEC is violated. Here, $b = 1.4, c = 0.5$

2.2 Energy conditions

In this subsection, we shall analyze the energy conditions corresponding to the metric in Eq. (3). Since most of the wormhole spacetimes discussed in the literature violate the energy conditions, it is important to check this out for our metric as well.

The EM tensor can be calculated from the Einstein equations $G_{\mu\nu} = T_{\mu\nu}$. Since our considered geometry does not possess any event horizon, the components of the energy momentum tensor, given by $\rho = -T_t^t, p_r = T_r^r, p_\theta = T_\theta^\theta = T_\phi^\phi$ are valid for all values of the coordinate r for which the metric is valid i.e., for the WH branch the range is $-\infty < r < \infty$, and given for the NS branch by $\sqrt{b^2 - c^2} \leq r < \infty$. It is enough to check if the null energy condition (NEC) is violated because if that is the case, then all the other energy conditions are violated as well. The NEC in this case is given from $\rho + p_r \geq 0$ and $\rho + p_\theta \geq 0$. Before proceeding, we recall that NEC is violated for SV spacetimes for all the values of the parameter c, whereas the JNW metric satisfies the NEC everywhere.

In Figs. 6 and 7, we have plotted $\rho + p_r$ for both the WH and NS branch of the metric of Eq. (3), with the parameters indicated in the respective captions. As can be seen, the WH branch violates the NEC everywhere, while for the NS branch, by decreasing the value of γ, this condition can be satisfied for all values of r. In this case only we need to check the second condition also. In Fig. 8, we have plotted the quantity $\rho + p_\theta$ for the same parameter values as in Fig. 7, and as can be seen, the plot with $\gamma = 0.25$ satisfies the condition $\rho + p_\theta > 0$ as well. Thus we conclude that, in contrast with the SV solution, for sufficiently small values of γ, the NEC can be made to be satisfied here.

It remains to check whether the solutions in the NS branch which satisfy the NEC (e.g. the red curves in Figs. 7 and 8) satisfy other energy conditions such as the weak energy conditions and the strong energy conditions as well. We have checked that these solutions in the NS branch satisfy the other energy conditions as well. Thus in the NS branch of the SV-JNW spacetime at least one set of solutions can be found which satisfies all the standard energy conditions for some particular values of the parameters.

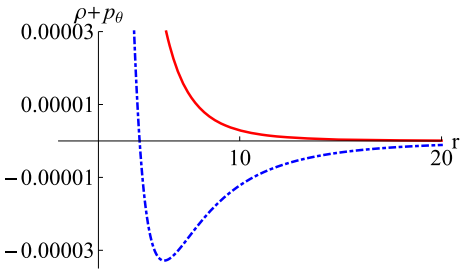

Fig. 8 $\rho + p_\theta$ for the NS branch. The solid red curve is for $\gamma = 0.25$ and the dashed blue curve is for $\gamma = 0.85$. Here, $b = 1.4$, $c = 0.5$

2.3 Source of the SV-JNW solution

An explanation of the above behavior of the energy momentum tensor and hence the NEC can be given by the following general considerations, as well as finding out the source of the SV-JNW metric following [41,49] (see also [42]). In this section we shall once again concentrate only on the branch $\gamma < 1$. We start by considering the following general static spherically symmetric line element

$$ds^2 = -\mathcal{A}(r)\mathrm{d}t^2 + \mathcal{A}^{-1}(r)\mathrm{d}r^2 + \mathcal{B}^2(r)\mathrm{d}\Omega^2. \tag{14}$$

Assuming that this metric satisfies the Einstein equations of the form $G^\mu_\nu = T^\mu_\nu$ we obtain,

$$G^t_t - G^x_x = 2\mathcal{A}(r)\frac{\mathcal{B}''(r)}{\mathcal{B}(r)} = -(\rho + p_r). \tag{15}$$

Since for the branch of the SV-JNW spacetime we are considering, $\mathcal{A} > 0$ for ranges of r for which the metric is valid, the sign of second derivative of the areal radius determines whether the condition $(\rho + p_r) \geq 0$ is satisfied or not. For our solution we calculate the required quantity to be

$$\frac{\mathcal{B}''(r)}{\mathcal{B}(r)} = \frac{4c^2(c^2+r^2) + b^2(2c^2 + r^2(-1+\gamma))(1+\gamma) - 2bc^2\sqrt{c^2+r^2}(3+\gamma)}{4(c^2+r^2)^2(b-\sqrt{c^2+r^2})^2}. \tag{16}$$

Now it can be easily seen that with $\gamma < 1$, depending on the relative values of the parameters b and c this quantity can be positive or negative. In particular for the WH branch with $c > b$ this quantity is everywhere positive for the entire respective range of r, while for the NS branch with $b > c$ the sign can be both positive or negative depending on the value of γ. With given values of $b > c$, for relatively higher values of γ, a range of r coordinate can be found where this quantity is positive – thereby violating the NEC.

These observations can be more clearly understood by finding out the source of the SV-JNW spacetime. In the context of the SV regularization of the Schwarzschild solution as it was recently shown in [41], a combination of a scalar field $\phi(r)$ and a nonlinear electromagnetic field, both minimally coupled to gravity, can act as a source of such spacetimes (see also [42]). Furthermore, in [49] it was also established that the scalar and nonlinear electromagnetic field can act as the source of an arbitrary static spherically symmetric metric. In this section we find out the scalar field and the nonlinear electrodynamic (NED) field corresponding to the SV-JNW solution.

We consider the following matter action

$$\mathcal{S}_m = \int \sqrt{-g}d^4x\Big[-\frac{1}{2}h(\phi)\partial_\mu\phi\partial^\mu\phi - V(\phi) + \mathcal{L}(\mathcal{F})\Big], \tag{17}$$

which contains an action of a scalar field $\phi(r)$ and that of a nonlinear electromagnetic field $\mathcal{L}(\mathcal{F})$. Here $h(\phi)$ is a function of ϕ and $V(\phi)$ is the corresponding potential. The Lagrangian density of the NED field $\mathcal{L}(\mathcal{F})$ is written as a function of $\mathcal{F} = F_{\mu\nu}F^{\mu\nu}$, where the electromagnetic field tensor $F_{\mu\nu}$ is defined in terms of the vector potential in the usual way $F_{\mu\nu} = \partial_\mu A_\nu - \partial_\nu A_\mu$.

The energy–momentum tensor obtained by varying the above action contains two parts corresponding to the scalar field and the NED respectively: $T^\nu_\mu = \Phi^\nu_\mu[\phi] + N^\nu_\mu[F]$. Explicitly, these are given by

$$\Phi^\nu_\mu[\phi] = \frac{1}{2}h(\phi)\partial_\mu\phi\partial^\nu\phi - \delta^\nu_\mu\Big[\frac{1}{4}h(\phi)\partial_\sigma\phi\partial^\sigma\phi + \frac{V(\phi)}{2}\Big],$$
$$N^\nu_\mu[F] = 2\mathcal{L}_\mathcal{F}F_{\mu\sigma}F^{\mu\sigma} - \frac{1}{2}\delta^\nu_\mu\mathcal{L}(\mathcal{F}). \tag{18}$$

Here, we have used the notation $\mathcal{L}_\mathcal{F} = \frac{d\mathcal{L}(\mathcal{F})}{d\mathcal{F}}$.

Now assuming that $\phi = \phi(r)$ and the source of the electromagnetic field is a magnetic monopole of charge q_m, i.e. $F_{\theta\phi} = q_m \sin\theta$, the spherical symmetry of the system restricts the components of the above EM tensor to be

$$\Phi^\nu_\mu(r) = \frac{1}{4}h(r)\mathcal{A}(r)\phi'^2(r)\,\mathrm{diag}\big(-1, 1, -1, -1\big) - \delta^\nu_\mu\frac{V}{2},$$
$$N^\nu_\mu(r) = -\frac{1}{2}\,\mathrm{diag}\big(\mathcal{L}, \mathcal{L}, \mathcal{L} - 2\mathcal{F}\mathcal{L}_\mathcal{F}, \mathcal{L} - 2\mathcal{F}\mathcal{L}_\mathcal{F}\big). \tag{19}$$

Here the prime denotes a derivative with respect to r. Notice that here the invariant is given by $\mathcal{F} = 2q_m^2/\mathcal{B}^4(r)$. Using the Einstein equation $G^{nu}_\mu = T^\nu_\mu$ we obtain the following relations between the metric components and the components of the EM tensor

$$G^t_t - G^r_r = T^t_t - T^r_r \;\rightarrow\; \frac{\mathcal{B}''(r)}{\mathcal{B}(r)} = -\frac{1}{4}h(r)\phi'^2(r),$$
$$G^t_t - G^\theta_\theta = T^t_t - T^\theta_\theta = -\mathcal{F}\mathcal{L}_\mathcal{F}, \tag{20}$$

where we have used Eq. (15) in the second expression of the first equation. We now use these equations to obtain the required scalar field and the nonlinear electromagnetic Lagrangian density.

First we obtain the function $h(r)$. Using the parametrization freedom of the scalar field we choose $\phi(r)$ to be (this

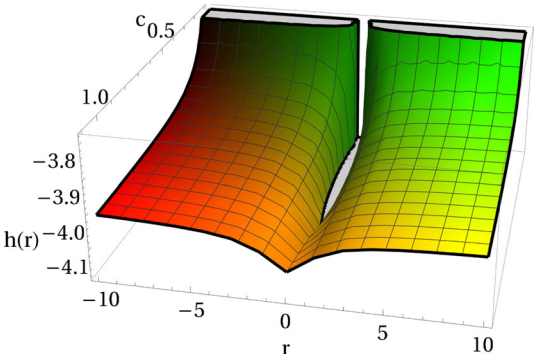

Fig. 9 Plot of the function $h(r)$ which determines the sign of the kinetic energy of the scalar field in the WH branch. Here $\gamma = 0.45$ and $b = 0.1$

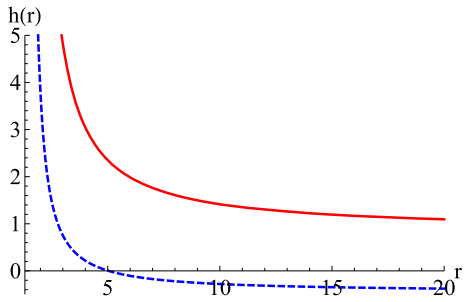

Fig. 10 Plot of the function $h(r)$ in the NS branch. The red curve is with $\gamma = 0.25$ and the blue curve is for $\gamma = 0.85$. For both the plots $b = 1.4$, $c = 0.5$

choice has been used in [41,49]),

$$\phi(r) = \arctan(r/c). \tag{21}$$

Substituting this form of the scalar field in the first equation of (20) along with the form of the areal radius $\mathcal{B}(r)$ for the metric in Eq. (3) we can obtain the functional dependence of $h(r)$. However the expression for it is lengthy and we do not provide it here, rather we will be interested the limiting behaviour of this functions at a few particular coordinate locations, namely $r \to 0$ and $r \to \pm\infty$. These are respectively given by

$$h(r)\Big|_{r\to 0} = -\frac{2(b-2c+b\gamma)}{b-c}, \quad \text{and}$$
$$h(r)\Big|_{r\to\pm\infty} = -\frac{4c^2+b^2(\gamma^2-1)}{c^2}. \tag{22}$$

Now it is easy to see that for the WH branch $b < c$, the function $h(r)$ is negative at the throat, indicating that the scalar field is phantom there. Furthermore, for this branch this function always remains negative for the entire range of the coordinate r, indicating that the scalar field is phantom in nature for the entire coordinate range of the WH branch. This is in contrast with the results obtained in [49], where a variation of the SV-JNW solution was constructed and it was shown that the function determining the sign of the kinetic energy can change sign depending on the value of the SV regularization parameter c. In Fig. 9, we have plotted the function $h(r)$ in the WH branch. From which it is easy to see that for the entire range of r, the function $h(r)$ does not change sign and is always negative.

On the other hand in the NS branch ($b > c$), similar to the behavior of the energy conditions, the nature of the scalar field depends on the parameter γ. In Fig. 10 we have plotted $h(r)$ for two values γ with fixed values of b and c in the NS branch. As can be easily seen for higher value of γ this function changes sign and hence the scalar field becomes phantom from canonical, whereas for a relatively lower value of γ the scalar field is always canonical.

Next, we can find out the NED Lagrangian density $\mathcal{L}(\mathcal{F}(r))$ as a solution of the following first order differential equation obtained from the second equation of (20):

$$\frac{d\mathcal{L}}{dr} = \frac{bc^2r(2\gamma+1)\left(1-\frac{b}{\sqrt{c^2+r^2}}\right)^{\gamma}\left(b(\gamma+1)-2\sqrt{c^2+r^2}\right)}{\left(c^2+r^2\right)^3\left(b-\sqrt{c^2+r^2}\right)^2}. \tag{23}$$

The solution for this equation is a smooth and positive function of r in both the WH and the NS branches of the SV-JNW solution. The explicit expression for $\mathcal{L}$ is cumbersome and we do not provide it here. Rather we note here that unlike the case of the (analogous) SV regularized Fisher solution presented in [49] this NED Lagrangian density does not reduce to zero for some specific value of γ. For the solution presented in [49] the density $\mathcal{L}$ is zero for $\gamma = 1/2$, so that source of the metric is only the scalar field.

3 The deformed JMN metric

As a second example of using the SV method to regularize naked singularities, we now study the SV modified version of the JMN metric, which is an equilibrium end state geometry of a realistic gravitational collapse model [30]. For a specific profile of energy density and tangential pressure, the spherically symmetric JMN metric is given by

$$ds^2 = -(1-M_0)\left(\frac{r}{r_b}\right)^{\frac{M_0}{1-M_0}}dt^2 + \frac{dr^2}{1-M_0} + r^2d\Omega^2. \tag{24}$$

Here r_b is a matching radius, and M_0 is related to the Schwarzschild mass, to which this metric can be matched smoothly. This metric represents an unstable equilibrium configuration of a collapsing star supported by a non zero tangential pressure and vanishing radial pressure.

As discussed in [30], if we confine our attention to the parameter region $0 < M_0 < 1$, then the metric does not

possess any event horizon, and there is a curvature singularity at $r = 0$. Thus, the range of the parameter M, to which we shall restrict ourselves here, is $0 < M_0 < 1$. It was also shown in the same work that in this geometry, there is at least one geodesic that can reach to an asymptotic observer that terminates at the singularity in the past, which points to the fact that the metric given in Eq. (24) is in fact a naked singularity. Our motivation in this section would be to check that whether this central singularity can removed by the SV modification, and study the resulting geometry. To this end, we first write down the resulting metric using the procedure of [16], which is given by,

$$ds^2 = -\big(1 - M_0\big)\left(\frac{\sqrt{r^2 + c^2}}{r_b}\right)^{\frac{M_0}{1-M_0}} \mathrm{d}t^2 + \frac{\mathrm{d}r^2}{1 - M_0} + \big(r^2 + c^2\big)\mathrm{d}\Omega^2. \tag{25}$$

Here as usual, c is a real positive quantity. The range of the radial coordinate is $r = -\infty$ to $r = \infty$, and the range of other coordinates remain same. We shall call this metric the SV-JMN solution. Now a little inspection shows that this metric actually is a traversable wormhole with a throat at $r = 0$ for all values of the parameter c. To see this, we first note that, as mentioned before, for $M_0 < 1$, the metric does not possess an event horizon. Secondly, the 'flaring out' condition of a traversable wormhole can be checked from considering the area of the two sphere $A(r) = (r^2 + c^2)$, which should satisfy the conditions $A'(r = r_0) = 0$, and $A''(r) = 2 > 0$. Hence the throat is the position of the minimum area, and the wormhole is two way traversable. It can also be checked that the Ricci scalar goes as $R \sim (r^2 + c^2)^{-2}$, and is finite everywhere including $r = 0$. Thus we conclude that the geometry in Eq. (25) is indeed a wormhole.

3.1 Photon motion in SV-JMN background

Now we briefly discuss the motion of massive and massless particles in the SV-JMN geometry, and compare them with those in the original JMN metric, the latter being studied in detail in [30,43]. Using the standard formula for the motion of photons in spherically symmetric spacetimes given in Eq. (11), we find the effective potential to be

$$V_{eff}(r) = \big(1 - M_0\big)\left(\frac{\sqrt{r^2 + c^2}}{r_b}\right)^{\frac{M_0}{1-M_0}} \left(\frac{C + L^2}{r^2 + c^2}\right), \tag{26}$$

and its derivative with respect to r is given by

$$V'_{eff}(r) = r\left(r^2 + c^2\right)^{\frac{5M_0-4}{2(1-M_0)}}. \tag{27}$$

Clearly, we have only one physically relevant solution for the photon sphere, namely $r = 0$, which is just the location of the throat of the WH geometry. The corresponding effective potential looks like the standard effective potential for the wormhole metric, when the throat acts as a position of the photon sphere – an example of which is already given in Fig. 3.

The components of the energy momentum tensor calculated from the metric in Eq. (25) are given by

$$\rho = \frac{M_0 r^2 + c^2\big(2M_0 - 1\big)}{\big(c^2 + r^2\big)^2}, \quad p_r = -\frac{c^2}{\big(c^2 + r^2\big)^2},$$
$$\text{and} \quad p_\theta = p_\phi = -\frac{M_0^2 r^2 + 2c^2\left(M_0^2 - 3M_0 + 2\right)}{4\big(c^2 + r^2\big)^2\big(M_0 - 1\big)}. \tag{28}$$

As can be seen directly from these expressions, the components are regular at $r \to 0$ and reduces to the JMN values in the limit $c \to 0$ (the role of negative pressure in gravitational collapse leading to naked singularities was investigated in [44]). In contrast to the original JMN spacetime, there is a non zero radial pressure here, which is always negative and vanishes at $c \to 0$ as it should. Since the original JMN metric represents the unstable equilibrium configuration of a gravitationally collapsing star with only the tangential components of pressure being non zero, it will be interesting to study whether our metric also represents an equilibrium configuration of a collapsing matter cloud with non zero radial pressure as well as a tangential pressure. We leave this for the future.

To check if the energy conditions are violated, it is enough in this case to check that NEC is violated for all values of the parameters. This can be readily seen from the expressions of ρ and p_r given above: since $M_0 < 1$, the quantity $\rho + p_r$ is always negative for sufficiently small values of r, and hence the NEC is violated.

3.2 Source of the SV-JMN

Next we shall find out the possible source of the SV-JMN solution following the method discussed in Sect. 2.3. First we notice that the line element of Eq. (25) written in the (t, r, θ, ϕ) coordinates is not of the form in Eq. (14). It is possible to make a coordinate transformation such that we can cast it as that of Eq. (14), however the resulting coordinates expressions are difficult manipulate analytically. Rather we work with the line element of Eq. (25) and modify the results of Sect. 2.3 suitably.

Here we need to write down the components of the EM tensor obtained from Eq. (18) for a general metric of the form

$$ds^2 = -\mathcal{A}_1(r)\mathrm{d}t^2 + \mathcal{A}_2^{-1}(r)\mathrm{d}r^2 + \mathcal{B}^2(r)\mathrm{d}\Omega^2. \tag{29}$$

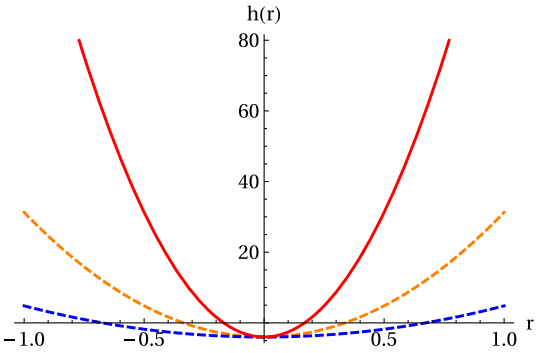

Fig. 11 Plot of the function $h(r)$ for the regular JMN metric. Here $M = 0.15$, and $c = 0.05$ (red), $c = 0.1$ (orange), and $c = 0.2$ (blue) respectively

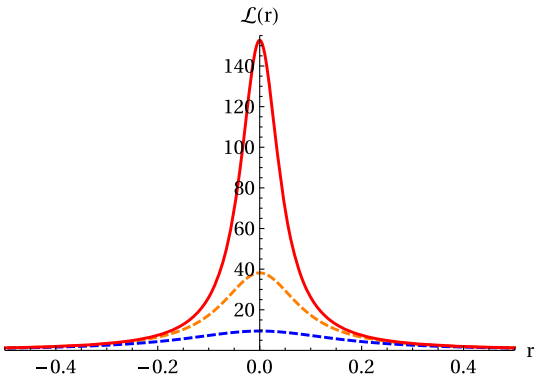

Fig. 12 Plot of the NED Lagrangian density $\mathcal{L}(\mathcal{F}(r))$ for the regular JMN metric. Here $M = 0.15$, and $c = 0.05$ (red), $c = 0.1$ (orange), and $c = 0.2$ (blue) respectively

It can be easily checked that the EM tensor corresponding to the scalar part in Eq. (19) changes to

$$\Phi^{\nu}_{\mu}(r) = \frac{1}{4}h(r)\mathcal{A}_2(r)\phi'^2(r)\,\mathrm{diag}\big(-1,1,-1,-1\big) - \delta^{\nu}_{\mu}\frac{V}{2}, \tag{30}$$

Using the same procedure outlined in Sect. 2.3 and using Eq. (21) as the choice of the scalar field we obtain the expression for the function $h(\phi)$ to be

$$h(\phi) = \frac{2M_0\tan\phi^2}{1-M_0} - 4 = \frac{2M_0r^2}{c^2(1-M_0)} - 4. \tag{31}$$

Close to the throat, $h(r)$ is always negative, indicating that the scalar field is phantom near the throat. On the other hand at $r \to \pm\infty$ this diverges, so that the for some intermediate value of r the scalar field changes its nature.

Plots of the function with respect to r for different values of c are shown in Fig. 11. As can be seen, this function is negative very close to the WH throat at $r = 0$ for any values of the constant c. However by decreasing the constant c sufficiently, the negative part of the function $h(r)$ can be confined in a very small region around the throat.

In this case we can also provide the analytic expression for the NED Lagrangian density. Written as a function of r this is given by

$$\mathcal{L}(r) = \frac{M_0\Big(c^2(9M_0-10)+2(3M_0-4)r^2\Big)}{4(c^2+r^2)^2(M_0-1)}. \tag{32}$$

This function is plotted in Fig. 12 for different values c. We see that this is maximum near the throat and goes to zero at $r \to \pm\infty$.

Finally, we point out that the SV-JMN metric we have constructed above is valid for all values of r, namely, $-\infty < r < \infty$. However, the JMN configuration was constructed to be the interior of collapsing matter distribution, matched with an exterior Schwarzschild solution of mass $M_{sch} = M_0 r_b/2$, where the matching radius $r = r_b$. It may be worth mentioning that by redefining the constant r_b as $\sqrt{r_b^2+c^2}$, the metric in Eq. (25) can be matched with an exterior SV metric of the form

$$ds^2 = -\left(1-\frac{M_0\sqrt{r_b^2+c^2}}{\sqrt{r^2+c^2}}\right)\mathrm{d}t^2 + \left(1-\frac{M_0\sqrt{r_b^2+c^2}}{\sqrt{r^2+c^2}}\right)^{-1}\mathrm{d}r^2 + \left(r^2+c^2\right)\mathrm{d}\Omega^2. \tag{33}$$

Here $M_{sv} = M_0\sqrt{r_b^2+c^2}/2$ with M_{sv} being the mass appearing in the SV metric. Obviously the constant r_b appearing here is different from the one in Eq. (25), and we also note that for a given $M_{sch} = M_{sv}$, the values of r_b are different for JMN and SV-JMN metrics. In particular, for a given value of $M_{sch} = M_{sv} = M$, the SV-JMN solution has smaller matching radius than its JMN cousin. Since the metric outside is SV (rather than Schwarzschild), we expect the properties of accretion disks corresponding to this model to be different from those discussed in [30] and this might be interesting to investigate. Furthermore, it will be interesting to study the collapse of realistic matter with SV taken as the exterior to see whether SV-JMN solution discussed above arises as an equilibrium configuration. We hope to return to this problem in a future work.

4 Quasinormal modes of the regularized JNW metric

Having investigated properties of the regularized JNW metric in Sect. 2, we now address the important question of the stability of the JNW metric, focusing on the physically interesting wormhole branch (represented by the parameter ranges $b < c$ and $\gamma < 1$). Specifically, in this section we calculate the QNMs of the wormhole branch of the solution. As is well known, QNMs are the eigenmodes of perturbations of spacetime. In general, QNMs are complex values, where the

real parts give the oscillation frequencies, while the imaginary parts signify the damping rates. Hence, for a dissipative solution like a black hole or wormhole, positivity of the imaginary part of the eigenmodes would indicate instability. QNMs have long been used to prove stability of black hole spacetimes (see, for example, [50–52]) and recently have been used to investigate stability of wormholes as well in several works [62–64,67].

Before moving on to calculating the QNMs in the wormhole background, it must be stressed that the solution we are considering is generically not vacuum. So, legitimate concern might appear about the justification of writing the free Klein–Gordon type of equation for the matter field in this background. However, to a first approximation, it is reasonable to assume negligible interaction between the matter sector of the theory and the test scalar field used to study the spectra as is usually done in the literature [62,67]. Below we discuss the form for the effective potential for the scalar field in the Schrödinger type Eq. (39) for the SV-JNW background.

We begin by considering a scalar perturbation in the regularized JNW background, whose form is given by,

$$\frac{1}{\sqrt{-g}}\partial_\mu\left(\sqrt{-g}g^{\mu\nu}\partial_\nu\Psi(t,r,\theta,\phi)\right)=0. \tag{34}$$

Using the explicit form of the metric in Eq. (29), this equation can be written as (with $\mathcal{A}_1(r)=\mathcal{A}_2(r)=f(r)$)

$$\begin{aligned}&\frac{\partial_t^2\Psi}{f(r)}+\frac{1}{\mathcal{B}^2(r)}\Big(\partial_r(\mathcal{B}^2(r))f(r)\partial_r\Psi\\&+\mathcal{B}^2(r)f'(r)\partial_r\Psi+\mathcal{B}^2(r)f(r)\partial_r^2\Psi\Big)\\&+\frac{1}{\mathcal{B}^2(r)}\left(\frac{1}{\sin\theta}\partial_\theta\sin\theta\partial_\theta\Psi+\frac{1}{\sin^2\theta}\partial_\phi^2\Psi\right)=0.\end{aligned} \tag{35}$$

Since the regular JNW metric above is spherically symmetric, the scalar field can be assumed to be of the form

$$\Psi(t,r,\theta,\phi)=\frac{\psi(t,r)}{\mathcal{B}(r)}Y_{lm}(\theta,\phi), \tag{36}$$

where $Y_{lm}(\theta,\phi)$ represent spherical harmonic function, and $\psi(t,r)$ is the function of radial coordinate t,r. Substituting Eq. (36) in Eq. (35), after a separation of variables we arrive at

$$\frac{\partial^2\psi(r,t)}{\partial t^2}-\frac{\partial^2\psi(r,t)}{\partial r_*^2}+V(r)\psi(r,t)=0, \tag{37}$$

here r_* is the tortoise coordinate, which is defined as,

$$dr_*=\frac{1}{f(r)}dr, \tag{38}$$

and ℓ is the separation constant for the angular parts. If we assume a harmonic time dependence $\psi(r,t)=u(r)e^{-i\omega t}$, Eq. (37) becomes

$$\frac{d^2u(r)}{dr_*^2}+\Big(\omega^2-V_{\rm scalar}(r)\Big)u(r)=0, \tag{39}$$

with the exact form of the effective potential written as

$$\begin{aligned}V_{\rm scalar}(r)=&\frac{f(r)\ell(\ell+1)}{\mathcal{B}^2(r)}+\frac{f^2(r)\partial_r^2\mathcal{B}(r)}{\mathcal{B}(r)}\\&+\frac{f(r)\partial_r f(r)\partial_r\mathcal{B}(r)}{\mathcal{B}(r)}.\end{aligned} \tag{40}$$

The final expression of Eq. (39) has the form of a one dimensional Schrodinger equation with potential $V_{\rm scalar}$. Here, we note that in a similar manner the effective potential for electromagnetic ($s=1$) and gravitational ($s=2$) perturbations can be expressed as,

$$V_s(r)=f(r)\left[\frac{\ell(\ell+1)}{\mathcal{B}^2(r)}+\frac{(1-s^2)}{\mathcal{B}(r)}\Big(f(r)\partial_r^2\mathcal{B}(r)+\partial_r f\partial_r\mathcal{B}(r)\Big)\right]. \tag{41}$$

Note that in the above equation, putting $s=0$ would result in the effective potential for scalar perturbation. Henceforth, we shall mainly concentrate our analysis on the scalar field perturbation, since results for the electromagnetic and gravitational cases are not qualitatively different.

The plot for the effective potential $V_{\rm scalar}$ of the scalar field is given in Fig. 13 for various values of the parameters b, c, γ and ℓ. Panels (a) and (b) show the variation of $V_{\rm scalar}$ versus r, whereas in panels (c) and (d), $V_{\rm scalar}$ has been plotted against r_*, which has been obtained by numerical integration. Panels (a) and (c) of Fig. 13 show that for several values of the parameters (all of which ensure that we are choosing the wormhole branch of the solution), the effective potential exhibits a single peak, with two turning points. Panels (b) and (d) show some parameter choices where a double peak is exhibited. This is similar to other wormhole solutions in the literature [67]. The figure also shows that $V(r,r_*\to\infty)\approx 0$ for the wormhole branch. From the wave equation, it is clear that asymptotically the solution takes the form $\Psi\approx e^{\pm i\omega t}$. This ensures that the physically relevant solutions are purely outgoing and incoming at infinity and the wormhole throat respectively.[2] The form of the effective potential suggests the use of the WKB method for calculating the QNMs of the wormhole. At the same time, panel (b) of Fig. 13 shows multiple peaks for the effective potential for several other parameter choices. However, it is important to note that this method would not be valid for calculating QNMs in case of the naked singularity because of the markedly different structure of the effective potential. Since the WKB method has been used extensively in the literature for calculating

[2] It is well known that the throat of the WH plays the same role as that of a BH event horizon in case of absence of any reflecting potential at $r_*\to-\infty$ [62].

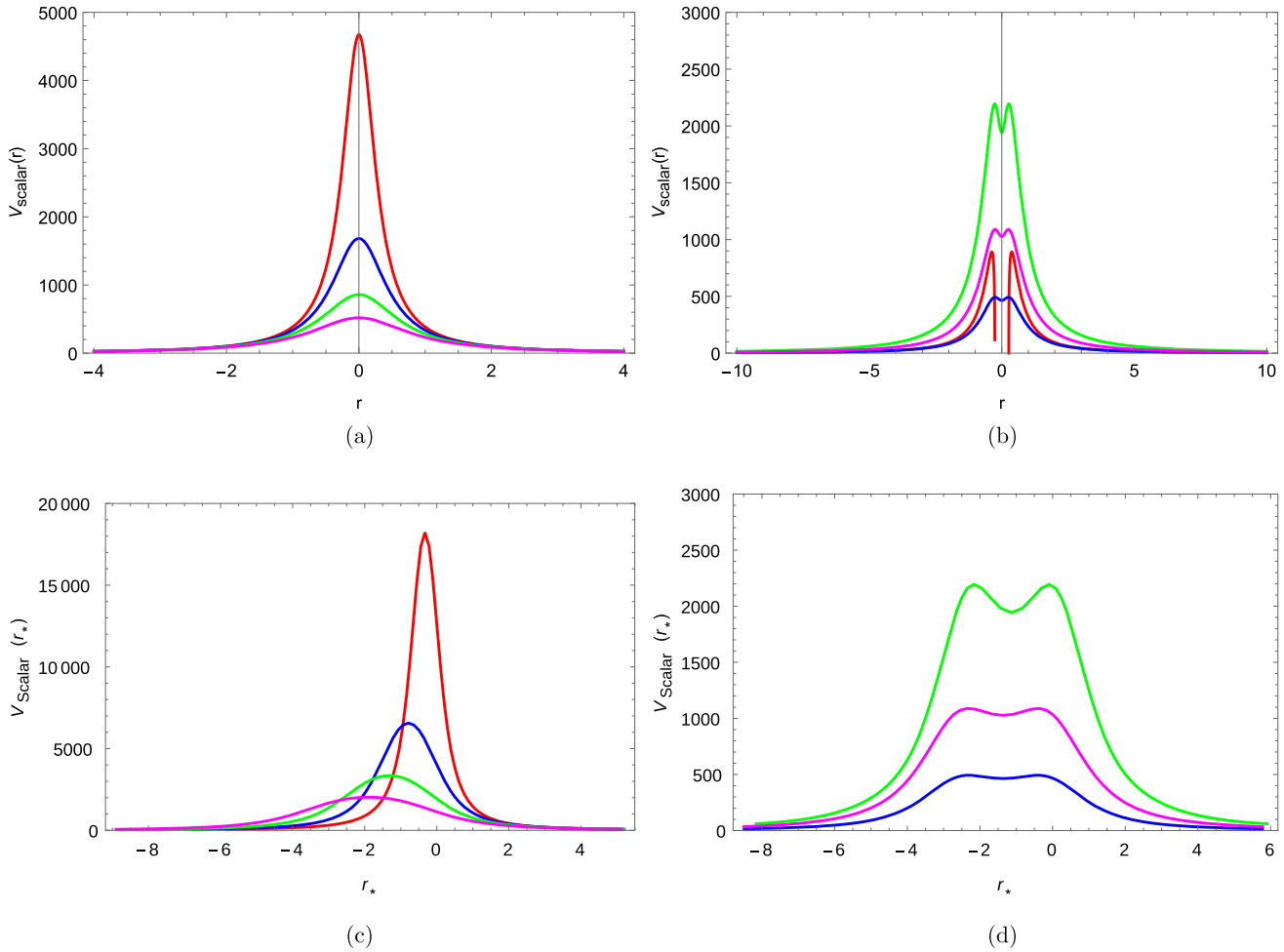

Fig. 13 Variation of the potential $V_{scalar}(r)$ against r and r_*. The red, blue, green and magenta curves denote $(b, c, \gamma, \ell) = (0.2, 0.3, 0.5, 20)$, $(0.4, 0.5, 0.5, 20)$, $(0.6, 0.7, 0.5, 20)$, $(0.8, 0.9, 0.5, 20)$ respectively in panel **a** and $(0.4, 0.3, 0.7, 20)$, $(0.4, 0.5, 0.9, 20)$, $(0.3, 0.4, 1.1, 40)$, $(0.4, 0.5, 0.9, 30)$ in panel **b**. The parameter choices for the red curve in panel **b** ensure that it denotes the potential for the naked singularity solution. In panels **c** and **d**, the same colour coding is followed as in **a** and **b** respectively. Note that in panel **d**, the curve corresponding to the naked singularity is not given because of the difficulty in performing the numerical integration for $r_*(r)$

QNMs (see, for example [51,52]), we shall not describe it here. Briefly, the expression for the QNMs obtained by this method is,

$$\omega^2 = \left[V_0 + \sqrt{-2V_0''}\,\Lambda(n) - i\left(n + \frac{1}{2}\right)\sqrt{-2V_0''}\,(1 + \Omega(n))\right], \tag{42}$$

with

$$\Lambda(n) = \frac{1}{\sqrt{-2V_0''}}\left[\frac{1}{8}\left(\frac{V_0^{(4)}}{V_0''}\right)\left(\frac{1}{4} + \alpha^2\right) - \frac{1}{288}\left(\frac{V_0'''}{V_0''}\right)^2\left(4 + 60\alpha^2\right)\right], \tag{43}$$

and

$$\begin{aligned}\Omega(n) = \frac{1}{-2V_0''}\Bigg[&\frac{5}{6912}\left(\frac{V_0'''}{V_0''}\right)^4\left(77 + 188\alpha^2\right) \\ &- \frac{1}{384}\left(\frac{V_0'''^2 V_0^{(4)}}{V_0''^3}\right)\left(51 + 100\alpha^2\right) \\ &+ \frac{1}{2304}\left(\frac{V_0^{(4)}}{V_0''}\right)^2\left(67 + 68\alpha^2\right) \\ &+ \frac{1}{288}\left(\frac{V_0''' V_0^{(5)}}{V_0''^2}\right)\left(19 + 28\alpha^2\right) \\ &- \frac{1}{288}\left(\frac{V_0^{(6)}}{V_0''}\right)\left(5 + 4\alpha^2\right)\Bigg].\end{aligned} \tag{44}$$

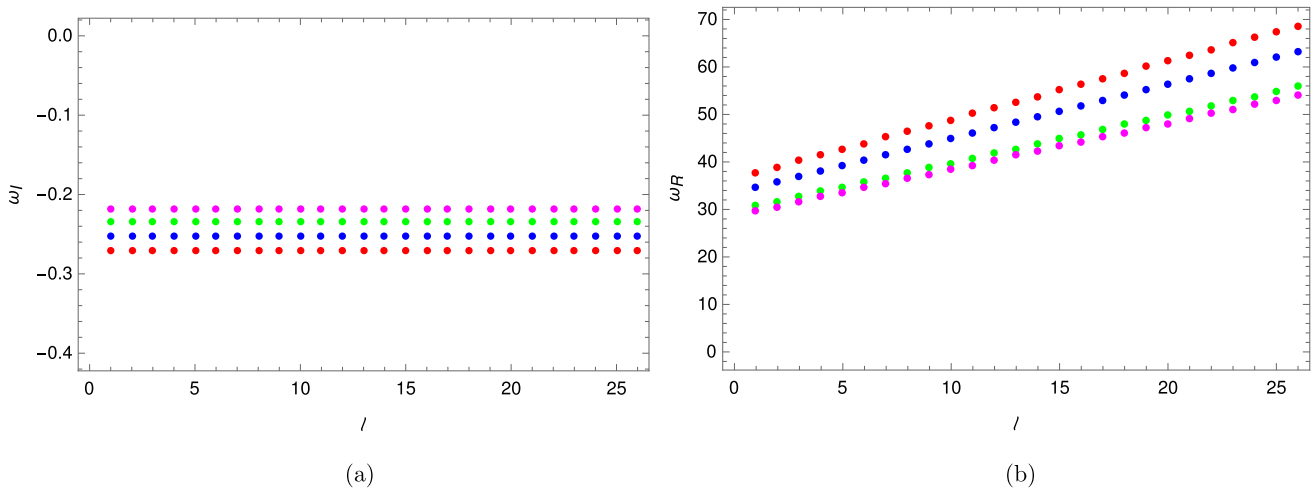

Fig. 14 Variation of real and imaginary parts of ω ($n = 0$) against ℓ. Here, $b = 0.4$, $c = 0.5$ and $\gamma = 0.2, 0.3, 0.4, 0.5$ for the red, blue, green and magenta curves respectively

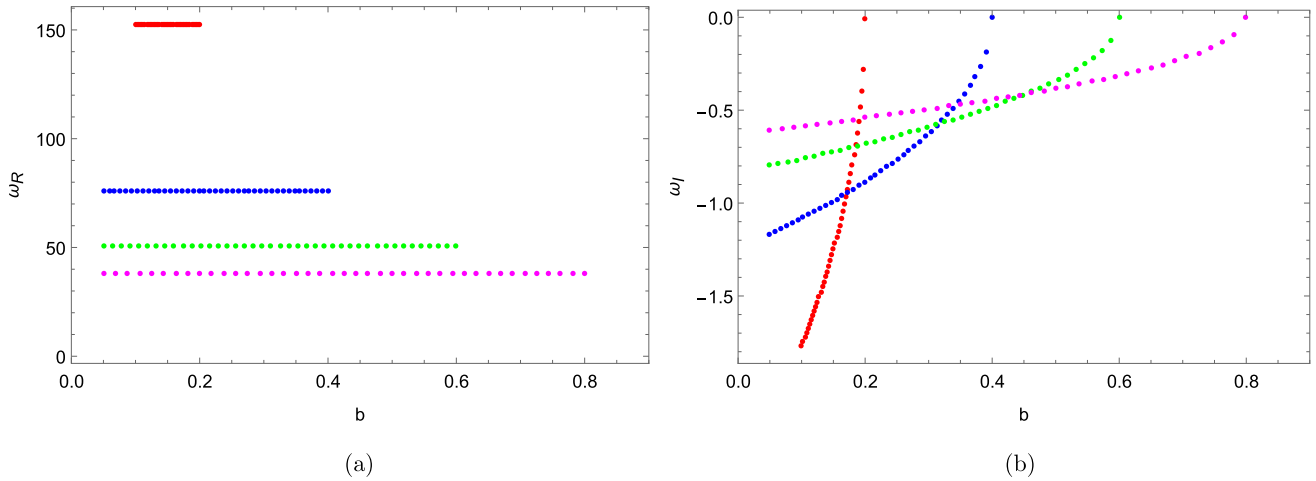

Fig. 15 Variation of the real and imaginary part of ω ($n = 0$) against b. Here c, $\gamma = 0.5$ and $\ell = 30$ are held constant. The red, blue, green and magenta curves denote $c = 0.2, 0.4, 0.6, 0.8$ respectively

Here, α and V_0^n are given by

$$\alpha = n + \frac{1}{2}, \quad V_0^n = \frac{d^n V}{dr_*^n}\Big|_{r_*=r_*(r_{max})}, \tag{45}$$

with $n = 0, 1, 2\ldots$ In the above equation, the prime denotes differentiation with respect to r_*, which can be translated to differentiation with respect to r by use of the chain rule. Also, $V_0 \equiv V_{scalar}(r_0)$, where $r_* = r_0$ denotes the extremum of the potential.

We shall primarily be interested in the fundamental $n = 0$ frequency. Before employing the WKB method to calculate QNMs, it is necessary to ensure that, for the parameter values chosen, the effective potential exhibits only a single peak, thus ensuring two turning points. For example, this would include Fig. 13a, c, and would rule out the parameter choices corresponding to Fig. 13b, d. It is instructive to plot the real and imaginary parts of ω against ℓ. This is shown in Fig. 14a, b, from which it is clear that the higher values of l do not necessarily dominate the spectrum of QNMs due to the magnitude of the imaginary component of the QNMs not appreciably varying as ℓ is changed.

It is also interesting to study the effect of the variation of the parameters b and c on the QNMs. This is physically interesting because it may be recalled from Sect. 2 that the parameter regime $b > c$ would ensure that the solution would be a naked singularity instead of a wormhole. Hence, by keeping c constant and varying b such that $b < c$, it would be possible to check whether the QNMs indicate any change in the wormhole solution as we get closer to the naked singularity branch.[3]

[3] It is important to reiterate that the QNMs of the naked singularity branch cannot be calculated by the WKB method (see Fig. 13b).

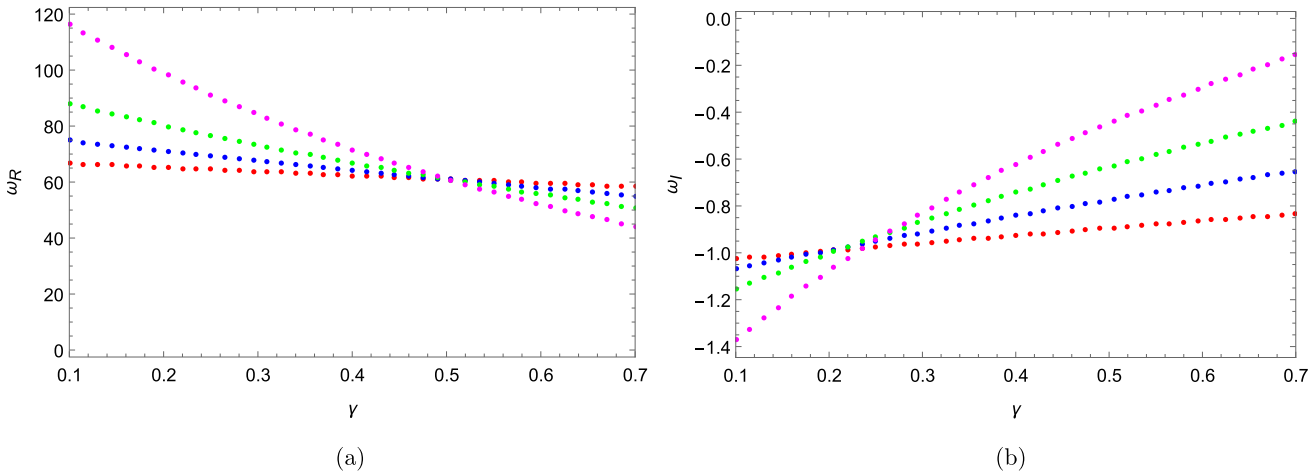

Fig. 16 Variation of the real and imaginary part of ω ($n = 0$) against γ. The red, blue, green and magenta curves denote $b = 0.1, 0.2, 0.3, 0.4$ respectively, with $c = 0.5$ and $\ell = 30$ in all cases

This analysis is done in Fig. 15, where for different values of the parameter c, we have varied b to approach very close to c, with γ and ℓ kept constant. It may be observed from Fig. 15b that, irrespective of the values of the parameters chosen, the wormhole solutions becomes less stable as the naked singularity limit $b \to c$ is approached. This is physically interesting, as it may have implications for the stability and existence of naked singularities in general.

Lastly, we investigate the variation of the real and imaginary parts of QNMs with γ in Fig. 16. It can be clearly seen that the stability of the wormhole solution decreases with increasing γ when the parameters b, c and ℓ are constant. It should be noted that with increasing γ and ℓ, the scalar potential exhibits a double peak. As a result, we have confined the analysis to a suitable range of parameters where the potential shows a single extremum.

Before moving on to the discussions, it may be noted that the QNMs of the regularized JMN solutions can also be studied in the same way. However, since this spacetime has only a wormhole branch in the parameter space, the results should be similar to the standard wormhole metrics available in the literature [65–67].

5 Discussions and outlook

In this paper, we have constructed and studied the properties of two classes of spacetimes, following the Simpson–Visser method of regularizing a singular metric. In the first set of metrics, we have found a new class of spacetimes that arise as deformations of the well known JNW naked singularity. By using the SV procedure, we arrive at a novel spacetime that interpolates between a naked singularity and a wormhole depending on the associated parameter space. While the WH nature of the original JNW metric for $\gamma > 1$ was already known in the literature, here we have shown that the SV-JNW metric has a WH branch even for $\gamma < 1$. We have also studied the observational aspects of the metric in terms of the effective potential for photon motion in detail. Interestingly, whereas in the case of the original JNW metric, the allowed range of the parameter γ is $0.5 \leq \gamma \leq 1$ for light rays to form a photon sphere, in the SV-JNW metric, even if $\gamma \leq 0.5$ photons can form unstable orbits depending on the other parameters of interest, thereby making this metric very different from that of JNW.

Next, we have used the JMN metric as a starting point, which arises as an end state of collapse involving tangential pressures, and applied the SV procedure. To this end we have exemplified another class of metrics which solely represents a wormhole for arbitrarily small values of the SV parameter. Finally, we have carried out an analysis of the QNMs of the modified JNW spacetime concentrating mainly on the wormhole branch. Using the standard WKB analysis, we have shown that the higher values of l do not always have a significant contribution to the QNM spectrum. On the other hand, our analysis suggests that as the parameter is varied in the model to approach the NS branch, the WH solution tends to be more unstable, which points towards some generic instability in the full NS domain.

We have in this paper restricted ourselves to spherically symmetric models of black bounce spacetimes, though the rotating versions of these have also appeared in the literature [45–48]. It would interesting to extend our models to include rotation, which we leave for a further study.

Data Availability Statement This manuscript has no associated data or the data will not be deposited. [Authors' comment: This is a theoretical work, and no external data have been used.]

Funded by SCOAP[3]. SCOAP[3] supports the goals of the International Year of Basic Sciences for Sustainable Development.

References

1. S. Carroll, *Spacetime and Geometry* (Pearson, London, 2004)
2. R. Penrose, Riv. Nuovo Cim. **1**, 252–276 (1969)
3. M. Visser, *Lorentzian Wormholes: From Einstein to Hawking* (AIP Press, Woodbury, 1995)
4. P. Kanti, B. Kleihaus, J. Kunz, Phys. Rev. Lett. **107**, 271101 (2011)
5. R. Shaikh, Phys. Rev. D **92**, 024015 (2015)
6. G. Antoniou, A. Bakopoulos, P. Kanti, B. Kleihaus, J. Kunz, Phys. Rev. D **101**(2), 024033 (2020)
7. R. Shaikh, S. Kar, Phys. Rev. D **94**(2), 024011 (2016)
8. A. Övgün, K. Jusufi, İ Sakallı, Phys. Rev. D **99**(2), 024042 (2019)
9. I. Sakalli, A. Ovgun, Astrophys. Space Sci. **359**(1), 32 (2015)
10. T. Damour, S.N. Solodhukin, Phys. Rev. D **76**, 024016 (2007)
11. J.M. Bardeen, Non-singular general relativistic gravitational collapse, in *Proceedings of International Conference GR5* (Tbilisi, USSR, 1968), p. 174
12. H. Maeda, JHEP **11**, 108 (2022)
13. R. Casadio, A. Giusti, J. Ovalle, Phys. Rev. D **105**(12), 124026 (2022)
14. A. Simpson, M. Visser, J. Cosmol. Astropart. Phys. **2019**, 042 (2019)
15. A. Simpson, P. Martin-Moruno, M. Viser, Class. Quantum Gravity **36**, 145007 (2019)
16. E. Franzin, S. Liberati, J. Mazza, A. Simpson, M. Visser, JCAP **07**, 036 (2021)
17. P. Bambhaniya, S.K.K. Jusufi, P. S. Joshi, Phys. Rev. D **105**(2), 023021 (2022)
18. M. Guerrero, G.J. Olmo, D. Rubiera-Garcia, D.S.C. Gómez, JCAP **08**, 036 (2021)
19. M.Y. Ou, M.Y. Lai, H. Huang, Eur. Phys. J. C **82**(5), 452 (2022)
20. Y. Guo, Y.G. Miao, Nucl. Phys. B **983**, 115938 (2022)
21. Y. Yang, D. Liu, A. Övgün, Z.W. Long, Z. Xu, arXiv:2205.07530 [gr-qc]
22. M.E. Rodrigues, M.V. de S. Silva, arXiv:2204.11851 [gr-qc]
23. E.L.B. Junior, M.E. Rodrigues, Gen. Rel. Grav. **55**(1), 8 (2023)
24. N. Tsukamoto, Phys. Rev. D **105**(8), 084036 (2022)
25. S. Chakrabarti, S. Kar, Phys. Rev. D **104**(2), 024071 (2021)
26. H. Huang, J. Yang, Phys. Rev. D **100**(12), 124063 (2019)
27. J. Barrientos, A. Cisterna, N. Mora, A. Viganò, Phys. Rev. D **106**(2), 024038 (2022)
28. A.I. Janis, E.T. Newman, J. Winicour, Phys. Rev. Lett. **20**, 878 (1968)
29. K.S. Virbhadra, Int. J. Mod. Phys. A **12**, 4831–4836 (1997)
30. P.S. Joshi, D. Malafarina, R. Narayan, Class. Quantum Gravity **28**, 235018 (2011)
31. K.S. Virbhadra, S. Jhingan, P.S. Joshi, Int. J. Mod. Phys. D **6**, 357–362 (1997)
32. K.K. Nandi, A. Islam, J. Evans, Phys. Rev. D **55**, 2497–2500 (1997)
33. K.K. Nandi, Y.Z. Zhang, A.V. Zakharov, Phys. Rev. D **74**, 024020 (2006)
34. M.S. Morris, K.S. Thorne, Am. J. Phys. **56**, 395–412 (1988)
35. A. Simpson, arXiv:2104.14055
36. K.S. Virbhadra, C.R. Keeton, Phys. Rev. D **77**, 124014 (2008)
37. S. Sau, I. Banerjee, S. SenGupta, Phys. Rev. D **102**(6), 064027 (2020)
38. R. Shaikh, Phys. Rev. D **98**, 024044 (2018)
39. R. Shaikh, P. Banerjee, S. Paul, T. Sarkar, Phys. Lett. B **789**, 270 (2019)
40. R. Shaikh, P. Banerjee, S. Paul, T. Sarkar, JCAP **07**, 028 (2019)
41. K.A. Bronnikov, R.K. Walia, Phys. Rev. D **105**, 044039 (2022)
42. P. Cañate, Phys. Rev. D **106**(2), 024031 (2022)
43. R. Shaikh, P. Kocherlakota, R. Narayan, P.S. Joshi, Mon. Not. R. Astron. Soc. **482**(1), 52–64 (2019)
44. F.I. Cooperstock, S. Jhingan, P.S. Joshi, T.P. Singh, Class. Quantum Gravity **14**, 2195–2201 (1997)
45. J. Mazza, E. Franzin, S. Liberati, JCAP **04**, 082 (2021)
46. R. Shaikh, K. Pal, K. Pal, T. Sarkar, Mon. Not. R. Astron. Soc. **506**(1), 1229–1236 (2021)
47. H.C.D. Lima Junior, L.C.B. Crispino, P.V.P. Cunha, C.A.R. Herdeiro, Phys. Rev. D **103**(8), 084040 (2021)
48. Z. Xu, M. Tang, Eur. Phys. J. C **81**(10), 863 (2021)
49. K.A. Bronnikov, Phys. Rev. D **106**(6), 064029 (2022)
50. S. Chandrasekhar, S.L. Detweiler, Proc. R. Soc. Lond. A **344**, 441–452 (1975)
51. S. Iyer, C.M. Will, Phys. Rev. D **35**, 3621 (1987)
52. S. Iyer, Phys. Rev. D **35**, 3632 (1987)
53. E. Berti, V. Cardoso, A.O. Starinets, Class. Quantum Gravity **26**, 163001 (2009)
54. M.A. Cuyubamba, R.A. Konoplya, A. Zhidenko, Phys. Rev. D **98**(4), 044040 (2018)
55. F. Cremona, F. Pirotta, L. Pizzocchero, Gen. Relativ. Gravit. **51**(1), 19 (2019)
56. R.A. Konoplya, Phys. Lett. B **784**, 43–49 (2018)
57. M.S. Churilova, R.A. Konoplya, A. Zhidenko, Phys. Lett. B **802**, 135207 (2020)
58. K.A. Bronnikov, R.A. Konoplya, T.D. Pappas, Phys. Rev. D **103**(12), 124062 (2021)
59. İ Sakalli, S. Kanzi, Turk. J. Phys. **46**(2), 51–103 (2022)
60. E.C. Santos, J.C. Fabris, J.A. de Freitas Pacheco, arXiv:1903.04874 [gr-qc]
61. G. Dotti, R. Gleiser, J. Pullin, Phys. Lett. B **644**, 289–293 (2007)
62. S.W. Kim, Prog. Theor. Phys. Suppl. **172**, 21–29 (2008)
63. M.S. Churilova, Phys. Dark Universe **31**, 100748 (2021)
64. M.S. Churilova, R.A. Konoplya, Z. Stuchlik, A. Zhidenko, JCAP **10**, 010 (2021)
65. E. Franzin, S. Liberati, J. Mazza, R. Dey, S. Chakraborty, Phys. Rev. D **105**(12), 124051 (2022)
66. Y. Guo, C. Lan, Y.G. Miao, Phys. Rev. D **106**(12), 124052 (2022)
67. P. Dutta Roy, S. Kar, Phys. Rev. D **106**(4), 044028 (2022)